A pairwise nuclear fusion algorithm for particle-in-cell simulations: weighted particles at relativistic energies

D. Wu,[1,2] Z. M. Sheng,[1] W. Yu,[3] S. Fritzsche,[4] and X. T. He[1,2,5]

[1] *Institute for Fusion Theory and Simulation, Department of Physics, Zhejiang University, 310058 Hangzhou, China*
[2] *Collaborative Innovation Center of IFSA, Shanghai Jiao Tong University, Shanghai 200240, China*
[3] *Shanghai Institute of Optics and Fine Mechanics, 201800 Shanghai, China*
[4] *Helmholtz Institut Jena and Theoretisch Physikalisches Institut, Friedrich Schiller University, Jena, D-07743 Jena, Germany*
[5] *Key Laboratory of HEDP of the Ministry of Education, CAPT, and State Key Laboratory of Nuclear Physics and Technology, Peking University, 100871 Beijing, China*

(Dated: July 22, 2020)

A pairwise nuclear fusion algorithm for particle-in-cell simulations for arbitrarily weighted macro-particles at relativistic energies is proposed. When comparing with a recent work by D. P. Higginson et al [Journal of Computational Physics 388, 439 (2019)], our method is also fitted with the widely used Coulomb scattering algorithm by Takizuka and Abe, Nanbu and Yonemura, and Sentoku and Kemp. As the pairing scheme accounts for the entire macro-particle ensemble, the convergence of our method is therefore of quite robust. The algorithm is benchmarked in situations with like-particles, unlike-particles, thermonuclear plasmas, and beam-target fusion. It is shown that only $10 \sim 100$ macro-particle per cell is needed for the repeatability of fusion yields around 1%.

PACS numbers: 52.38.Kd, 41.75.Jv, 52.35.Mw, 52.59.-f

I. INTRODUCTION

The particle-in-cell (PIC) method [1] has established itself as a state-of-the-art method to understand kinetic phenomena in laboratory, astrophysical and fusion-relevant plasmas. Usually, the ions and electrons deviate from thermal equilibrium distributions. As the nuclear fusion cross section depends on the relative velocity between ions, such deviations from equilibrium can dramatically alter the emission of neutrons. Especially, for the neutron sources via intense laser interaction with pitcher-catcher target [2], intense ion beams at relativistic energies are produced by the non-linear laser plasma interactions, and their distributions significantly depart from thermal distributions. For this reason, the PIC method is currently maybe the only method for probing the dynamics of fusion reactions, e.g., neutron yield and spectra, alpha particle heating and self-generated electromagnetic fields. For computational and problem specific considerations, PIC simulations are often run with arbitrarily weighted particles. In a recent work, D. P. Higginson et al [3] proposed a method applying fusion reaction to PIC simulations with differing particle weights at non-relativistic energies. Such a method is based on a simple pair scheme: particles undergo a collision with only one pair and multiply by the number of unsampled pairs. However such a pairing scheme is in contrast to the series of works considering the entire macro-particle ensemble, for instance by Takizuka and Abe [4], Nanbu [5] and Yonemura, and Sentoku and Kemp [6]. Although significantly much involved, this pairing scheme, that accounting for the entire macro-particle ensemble, could ensure convergence of the simulation results by using small number of macro-particles. Furthermore, in many modern PIC codes, for example, EPOCH [7], PICLS [6] and LAPINS [8–11], the pairing scheme by Takizuka and Abe [4], Nanbu and Yonemura [5], and Sentoku and Kemp [6] has already been taken for Coulomb scattering simulations. Therefore a pairwise nuclear fusion algorithm that well fits with Coulomb scattering simulations and applicable for particles at relativistic energies is certainly on time and of great demand.

In this work, a pairwise nuclear fusion algorithm for arbitrarily weighted macro-particles at relativistic energies is proposed and benchmarked in situations with like-particles, unlike-particles, thermonuclear plasmas, and beam-target fusion. This method is well fitted with the widely used Coulomb scattering algorithm by Takizuka and Abe, Nanbu and Yonemura, and Sentoku and Kemp. As the used pairing scheme accounts for the entire macro-particle ensemble, the convergence of our method is therefore of quite robust. It is shown that only $10 \sim 100$ macro-particle per cell is needed for the repeatability of neutron yields around 1%.

II. NUCLEAR FUSION BETWEEN WEIGHTED PARTICLES AT RELATIVISTIC ENERGIES

We begin by introducing a pairwise nuclear fusion model for weighted particles at relativistic energies. Pairs of particles undergoing nuclear fusions are determined at random in each spatial cell. The pairing procedures between particles are identical to Takizuka and Abe [4], Nanbu and Yonemura [5], and Sentoku and Kemp [6]. Similar with a recent work by D. P. Higginson et al [3], energy and momentum exchanges via the nuclear fusion are calculated for each pair, performed in the center-of-momentum (CM) frame of the two particles. Here we revise the calculation by following strictly relativistic

kinematics in order to make the model applicable to the ultra-relativistic regime.

A. Center-of-momentum frame

The kinematics of a relativistic nuclear fusion between two particles with rest masses m_a and m_b, reduced momenta $\mathbf{u}_a = \gamma_a \mathbf{v}_a$ and $\mathbf{u}_b = \gamma_b \mathbf{v}_b$ is best calculated in the center-of-momentum frame of reference (CM). Note, currently it is not affected by the weight of the colliding particles. The velocity and relativistic factor of CM are

$$\mathbf{v}_{\rm CM} = \frac{m_a \mathbf{u}_a + m_b \mathbf{u}_b}{m_a \gamma_a + m_b \gamma_b} \tag{1}$$

and

$$\gamma_{\rm CM} = \frac{1}{(1 - \mathbf{v}_{\rm CM}^2)^{1/2}}. \tag{2}$$

The reduced momenta $\mathbf{u}_{a,b}$ as given in the laboratory frame of reference (LAB) are transformed into the CM frame by a Lorentz transformation,

$$\gamma_{a,\rm CM} = \gamma_{\rm CM}(\gamma_a - \mathbf{v}_{\rm CM} \cdot \mathbf{u}_a), \tag{3}$$

and

$$\mathbf{u}_{a,\rm CM} = \mathbf{u}_a + \frac{\gamma_{\rm CM} - 1}{\mathrm{v}_{\rm CM}^2}(\mathbf{v}_{\rm CM} \cdot \mathbf{u}_a)\mathbf{v}_{\rm CM} - \gamma_{\rm CM}\gamma_a \mathbf{v}_{\rm CM}. \tag{4}$$

It is easy to prove that $m_a \mathbf{u}_{a,\rm CM} = m_b \mathbf{u}_{b,\rm CM}$, and the velocities in CM frame are $\mathrm{v}_{a,\rm CM} = \mathbf{u}_a/\gamma_{a,\rm CM}$ and $\mathrm{v}_{b,\rm CM} = \mathbf{u}_b/\gamma_{b,\rm CM}$. The relative velocity between the two particles in the CM frame, required for the calculation of the cross section of nuclear fusion, is given by

$$\mathrm{v}_{\rm rel} = \frac{\mathbf{v}_{a,\rm CM} - \mathbf{v}_{b,\rm CM}}{1 - \mathbf{v}_{a,\rm CM} \cdot \mathbf{v}_{b,\rm CM}}. \tag{5}$$

For the calculation convenience of the momenta of fusion productions, we rotate the coordinate system of momentum space to the system in which the $u_{a,z,\rm CM}$-axis is aligned with the momentum vector $\mathbf{u}_{a,\rm CM}$. This transformation matrix is represented by

$$\mathbf{R} = \begin{bmatrix} \cos(\Theta)\cos(\Phi) & \cos(\Theta)\sin(\Phi) & -\sin(\Phi) \\ -\sin(\Phi) & \cos(\Phi) & 0 \\ \sin(\Theta)\cos(\Phi) & \sin(\Theta)\sin(\Phi) & \cos(\Theta) \end{bmatrix}, \tag{6}$$

and $[0, 0, u_{a,z,\rm CM}]^{\rm T} = \mathbf{R} \cdot [u_{a,x,\rm CM}, u_{a,y,\rm CM}, u_{a,z,\rm CM}]^{\rm T}$. Here Θ is the polar angle between $u_{a,z,\rm CM}$ -axis and the vector $\mathbf{u}_{a,\rm CM}$, and Φ is the azimuthal angle between $u_{a,x,\rm CM}$-$u_{a,y,\rm CM}$ plane.

B. Fusion probability

The two fusion reactant macro-particles, a and b, have the potential to undergo fusion and create two products, $\bar{c}$ and $\bar{d}$, with an energy gain, Q. The fusion probability for this interaction, P_{ab}, is given by

$$\mathrm{P}_{ab} = n_{\rm min}\sigma_{ab}\mathrm{v}_{\rm rel}\Delta t, \tag{7}$$

where $n_{\rm min}$ is the minimum density between particle species a and b, σ_{ab} is the cross section of nuclear fusion, and Δt is the time step of simulation. The cross-section of many fusion reactions have been fitted and simulated via various methods [12–16]. In general, theoretical and fitted values of the cross-sections usually present data using the kinetic energy in the CM frame, $E_r = m_r(\gamma_r - 1)$, where $m_r = m_a m_b/(m_a + m_b)$, and $\gamma_r = 1/(1 - \mathrm{v}_{\rm rel}^2)^{1/2}$. While experimentally, the cross section is usually tabulated as a function of the kinetic energy of the projectile $E_{a,\rm lab}$, with $E_{a,\rm lab} = (m_a + m_b)E_r/m_b$. Nuclear fusion yield for each pair of macro-particles is

$$\mathrm{Y}_{ab} = w_{\rm min}\mathrm{P}_{ab}, \tag{8}$$

where $w_{\rm min}$ is the minimum weight of macro-particles a and b. To increase the number of macro-products generated, D. P. Higginson et al [3] introduced the "fusion production multiplier", $F_{\rm mult}$; this increases the probability of fusion events, but decreases the weight of the products. In actual simulations, $F_{\rm mult}$ is a varying parameter, which depends on how many fusion produced macro-particles are required for data analysis.

C. Energies and momenta of fusion productions

Fusion products are produced in the CM frame, with the conservation of total energy and momenta. Since all of the products have the same weight, i.e. $w_{\rm min}/F_{\rm multi}$, the fusion process will conserve total energy and momentum perfectly. Here as the total energy includes the rest mass energy of particles, the kinetic energy, $E_{k,\rm CM}$, is not conserved, when rest mass energy is converted into kinetic energy, $E_{k,a,\rm CM} + E_{k,b,\rm CM} + Q = E_{k,\bar{c},\rm CM} + E_{k,\bar{d},\rm CM}$. Although the total momenta is fully conversed, calculating the magnitude of fusion production is not straightforward at relativistic energies. For non-relativistic energies, we have

$$m_{\bar{c}}^2 u_{\bar{c},\rm CM}^2 = m_{\bar{d}}^2 u_{\bar{d},\rm CM}^2 = \frac{2m_{\bar{c}}m_{\bar{d}}}{m_{\bar{c}} + m_{\bar{d}}}[m_r(\gamma_r - 1) + Q], \tag{9}$$

where $m_r(\gamma_r - 1)$ is the total kinetic energy of a and b in the CM frame, and here it can be easily proved that $m_r(\gamma_r - 1) = E_{k,a,\rm CM} + E_{k,b,\rm CM}$. However, at relativistic energies, the right part of above equation is changed to become $[2m_{\bar{c}}m_{\bar{d}}/(m_{\bar{c}} + m_{\bar{d}})][m_r(\gamma_r - 1) + Q + \alpha]$, where α has to be solved numerically. We here would suggest using golden section method [17] to solve α out, by literately decreasing the remains, $\delta_{\rm rem} = |m_{\bar{c}}[(1+u_{\bar{c},\rm CM}^2)^{1/2} - 1] + m_{\bar{d}}[(1 + u_{\bar{d},\rm CM}^2)^{1/2} - 1] - m_r(\gamma_r - 1) - Q|$.

As for the calculation of emission angles of fusion productions, $\bar{c}$ and $\bar{d}$, D. P. Higginson et al]citeHigginson

suggested an efficient random sampling method. However such a method only works for differential cross section fittings using a polynomial expansion in $\cos(\theta)$, where θ is the polar angle of the emission for particle $\bar{c}$. For a general differential cross section

$$\frac{d\sigma(E_{a,\mathrm{lab}},\theta)}{d\Omega} = \frac{d\sigma(E_{a,\mathrm{lab}},\theta=0)}{d\Omega} f(\theta), \tag{10}$$

we would suggest Box-Muller's algorithm [18] and Hormann and Leydold's algorithm [19]. When $f(\theta)$ is everywhere integrable, distribution function can be integrated to the cumulative density function $F = \int_0^\theta f(\theta)d\theta$ and the cumulative density function normalised such that $F(0) = 0$ and $\lim_{\theta\to\pi} F(\theta) = 1$. The cumulative density function is inverted:

$$\theta = F^{-1}(u);\ u \in (0,1), \tag{11}$$

When distribution function is not integrable, this process cannot be done analytically, and numerical methods of calculating the inverse cumulative distribution function must be used. It requires evaluations of $f(\theta)$; integration $F = \int_0^\theta f(\theta)d\theta$ and initial boundary conditions. The domain of $F^{-1}(\theta)$ is split into equally spaced sub-intervals and a cubic Hermite polynomial $H_i(u)$ is used to interpolate values of θ for given u, with $F(\theta)_i < u < F(\theta)_{i+1}$. For the entire interpolation process, the maximal acceptable error

$$\epsilon_u = \max|F(H_i(u)) - u|;\ u \in (u_i, u_{i+1}) \tag{12}$$

can be specified, and intervals are split until this is satisfied for every i. For some fusion reactions, currently only the total cross section as a function of projectile kinetic energy is measured experimentally. Then we would suggest to treat the emission of particles as isotropic with respect to the polar angle, θ, in the CM frame. Either way, the azimuthal angle ϕ is calculated as $\phi = 2\pi u$, with u uniformly distributed number between 0 and 1. These angles are applied to the first product, $\bar{c}$, to get its velocity in the CM frame,

$$\frac{\mathbf{u}_{\bar{c},\mathrm{CM}}}{u_{\bar{c},\mathrm{CM}}} = [\sin(\theta)\cos(\phi), \sin(\theta)\sin(\phi), \cos(\theta)]^{\mathrm{T}}. \tag{13}$$

From momenta conservation, the velocity of the second product, $\bar{d}$, in the CM frame is

$$\mathbf{u}_{\bar{d},\mathrm{CM}} = -\frac{m_{\bar{c}}}{m_{\bar{d}}}\mathbf{u}_{\bar{c},\mathrm{CM}}. \tag{14}$$

Then we invert the Matrix, $\mathbf{R}^{-1}$, which is a transpose of Matrix Eq. (6),

$$\mathbf{R}^{-1} = \begin{bmatrix} \cos(\Theta)\cos(\Phi) & -\sin(\Phi) & \sin(\Theta)\cos(\Phi) \\ \cos(\Theta)\sin(\Phi) & \cos(\Phi) & \sin(\Theta)\sin(\Phi) \\ -\sin(\Phi) & 0 & \cos(\Theta) \end{bmatrix}, \tag{15}$$

to obtain the unrotated momenta in the CM Frame, $\mathbf{u}_{\bar{c},\mathrm{CM}} = \mathbf{R}^{-1}\mathbf{u}_{\bar{c},\mathrm{CM}}$ and $\mathbf{u}_{\bar{d},\mathrm{CM}} = \mathbf{R}^{-1}\mathbf{u}_{\bar{d},\mathrm{CM}}$. Finally,

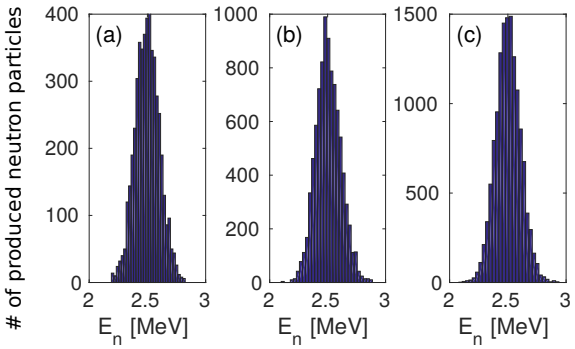

FIG. 1. (color online) Simulation results: the spectra of produced macro-neutrons for D(D,n)^{3}He fusion, (a)-(c) correspond to three different cases by placing 30, 60 and 90 macro D ions initially.

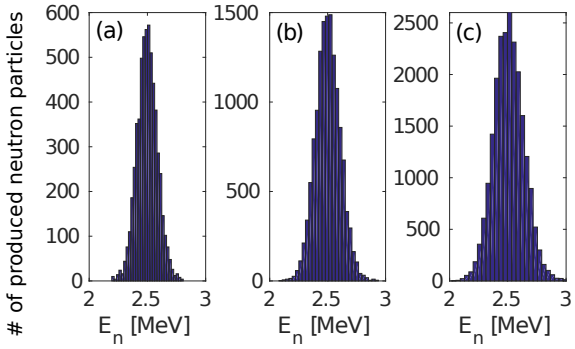

FIG. 2. (color online) Simulation results: the spectra of produced macro-neutrons for D(D,n)^{3}He fusion, (a)-(c) correspond to three different cases with initial temperatures, 3 keV, 5 keV, and 8 keV, respectively. In this benchmark, each cell is placed 90 macro-D-ions initially.

the particle momenta $\mathbf{u}_{\bar{c}}$ and $\mathbf{u}_{\bar{d}}$ in the laboratory frame are obtained by another Lorentz transformation,

$$\mathbf{u}_{\bar{c}} = \mathbf{u}_{\bar{c},\mathrm{CM}} + \frac{\gamma_{\mathrm{CM}}-1}{\mathrm{v}_{\mathrm{CM}}^2}(\mathbf{v}_{\mathrm{CM}}\cdot\mathbf{u}_{\bar{c},\mathrm{CM}}) + \gamma_{\mathrm{CM}}\gamma_{\bar{c},\mathrm{CM}}\mathbf{v}_{\mathrm{CM}},$$

and

$$\mathbf{u}_{\bar{d}} = \mathbf{u}_{\bar{d},\mathrm{CM}} + \frac{\gamma_{\mathrm{CM}}-1}{\mathrm{v}_{\mathrm{CM}}^2}(\mathbf{v}_{\mathrm{CM}}\cdot\mathbf{u}_{\bar{d},\mathrm{CM}}) + \gamma_{\mathrm{CM}}\gamma_{\bar{d},\mathrm{CM}}\mathbf{v}_{\mathrm{CM}}.$$

These calculations will be done for each binary pair.

TABLE I. Simulation results: the total yield of neutrons for D(D,n)^{3}He fusion, when changing the number of macro-D-ions for each cell initially. The initial temperature is 5 keV.

# of particles	10	20	30	40	50	60	70	80	90	100
real neutron yield	112	110	101	97	99	95	96	98	94	95

TABLE II. Simulation results: the FWHM of neutrons spectra for D(D,n)^{3}He fusion, when changing the initial temperature of D-ions.

keV	1	2	3	4	5	6	7	8	9	10
FWHM	50	110	120	150	180	200	220	240	255	265

TABLE III. Simulation results: the total yield of neutrons for D(T,n)^{4}He fusion, when changing the number of macro-D ions put for each cell initially. The initial temperature is 5 keV.

# of particles	10	20	30	40	50	60	70	80	90	100
real neutron yield	395	375	377	376	366	364	364	365	364	365

D. Paring method for weighted particles

The paring method is identical to the one described in Takizuka and Abe, Nanbu and Yonemura, and Sentoku and Kemp. We here approach this as a computational description and do not dive deep into the physics, as there are informative works on the subject.

Let $w_{a,i}$ represent the weight of the i-th particle of species a, and similarly, $w_{b,j}$ is for j-th particle of species b. The number density of each species in a cell is then given by

$$n_a = \sum_i^{N_a} w_{a,i},\ n_b = \sum_j^{N_b} w_{b,j}. \tag{16}$$

When the number of macro-particle in a cell, $N_a > N_b$, the number of binary pair is N_a, and the total number of pairs of real particles is

$$n_{ab} = \sum_i^{N_a} \frac{w_{a,i} w_{b,i}}{\max(w_{a,i} w_{b,i})}. \tag{17}$$

To make the total number of collision of real particles equal to the case with uniformly weighted particles, the time step fusion probability in Eq. (7) is corrected by multiplying a factor n_a/n_{ab}. This is a common time increment per real particle for each simulation grid at each simulation step. When $N_b > N_a$, n_b/n_{ab} is used instead.

In the case of species when a and b are identical, for example D(D,n)^{3}He, the number of pair is $N = N_a/2$ for even N_a, and $N_a = (N_a + 1)/2$ for odd N_a. The number of real particles that have collided is

$$n_{aa} = 2 \sum_i^{N} \frac{w_{2i-1} w_{2i}}{\max(w_{2i-1} w_{2i})}, \tag{18}$$

and then the multiplying factor becomes n_a/n_{aa}.

III. BENCHMARKS AND APPLICATIONS

To benchmark the algorithm, we present three cases, D(D,n)^{3}He thermonuclear fusion, T(D,n)^{4}He thermonuclear fusion, and D(D,n)^{3}He beam-target fusion, to illustrate the fidelity of the method when using large differences in weights and numbers of macro-particles per cell. The method described in this paper has already been implemented in the PIC code LAPINS. All of the tests were run with Coulomb scattering, particle motion and fields disabled. Thus the plasmas remained constant over all time and the fusion products were not able to heat the plasma.

A. D(D,n)^{3}He thermonuclear fusion

A simulation box with lengths $L_x = 1$ μm, $L_y = 1$ μm and $Lz = 10$ μm is divided into 10 cells along z directions, with each cell contains the same number of D-ions. The density of D-ions is 10^{24} cm^{-3}.

In the first benchmark, we assume the initial temperature of D-ions is 5 keV. After simulating for 3.3 fs, the spectra of produced macro-neutrons are displayed in Fig. 1. Here, Fig. 1 (a)-(c) correspond to three different cases by placing 30, 60 and 90 macro-D-ions initially. As we can see, the spectra of macro-neutrons are quite similar. Note, the weight of each macro-neutron shown in Fig. 1 is different, which significantly depends on how many macro-D-ions is placed initially. We display the total neutron yield by summarizing each macro-neutron multiplying its weight in Table. I. As we can see, the repeatability of fusion yields is around 1% when only $10 \sim 100$ macro-particle per cell is placed initially.

In the second benchmark, we fixed 90 macro D ions for all simulations by varying the initial temperature of D ions. Fig. 2, the spectra of produced macro-neutrons are displayed. Here, Fig. 2(a), (b) and (c) correspond to three cases with initial temperatures of 3 keV, 5 keV and 8 keV. As we can see, the width of neutron spectra is increasing when the initial temperature is increased. In Table. II, we have tabulated the FWHM of neutron spectra as a function of temperature. When comparing the benchmark results as reported by D. P. Higginson et al, great agreement is reached.

B. T(D,n)^{4}He thermonuclear fusion

As for the T(D,n)^{4}He thermonuclear fusion, the simulation setup is quite similar with D(D,n)^{3}He thermonuclear fusion, except that the same number of T-ions along with D-ions is placed in each cell. Here we only benchmark the total yield of neutron, with initial temperature fixed at 5 keV, by varying the initial number of macro-D- and T-particles per cell. Table. III shows the yield of neutron as a function of macro-particle numbers. As we can see, the repeatability of fusion yields is also around 1% when only $10 \sim 100$ macro-particle per cell is placed initially.

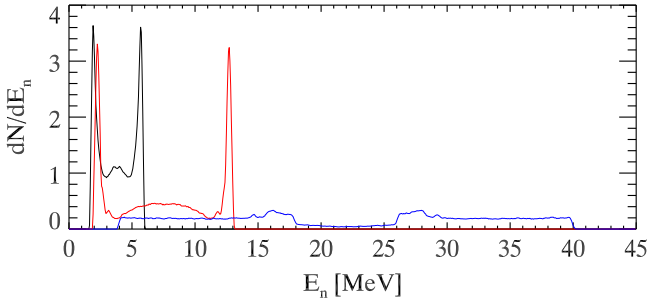

FIG. 3. (color online) Simulation results: the spectra of produced macro-neutrons for D(D,n)^{3}He fusion. Black, red and blue lines represent the cases when the initial projected (reduced) momentum is 0.05, 0.1 and 0.2, respectively.

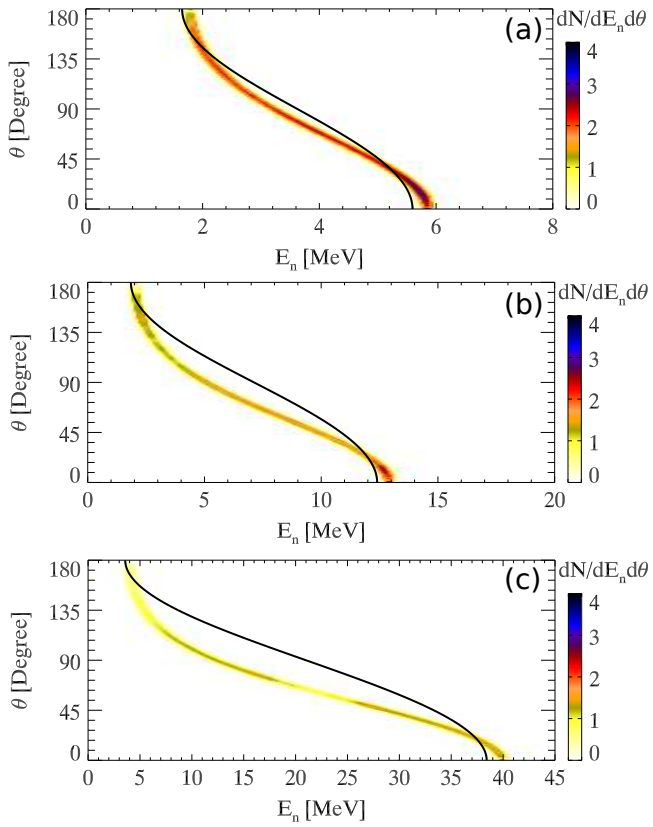

FIG. 4. (color online) Simulation results and analytical formula: the θ-E_n phase space plot of produced macro-neutrons for D(D,n)^{3}He fusion. Figure (a), (b) and (c) represent the cases when the initial projected (reduced) momentum is 0.05, 0.1 and 0.2, respectively. Here, Eq. (19) is plotted as the black curve on each figure.

C. D(D,n)^{3}He beam-target fusion

For beam-target fusion benchmark, the simulation setup is also similar as with the D(D,n)^{3}He thermonuclear fusion. Here, one group of D-ions is treated as stationary background with density 10^{24} cm^{-3}, and the other one with the same density is treated as projectiles. Three simulation cases, with projected (reduced) momentum of 0.05, 0.1 and 0.2, respectively, are run. In Fig. 3, we have displayed the spectra of produced neutron as a function of projectile momentum. Black, red and blue lines represent different cases when the initial projected (reduced) momentum is 0.05, 0.1 and 0.2, respectively. In Fig. 4, we also display the θ-E_n phase-space plot of produced macro-neutrons. Fig. 4 (a), (b) and (c) correspond to different cases when the initial projected momentum is 0.05, 0.1 and 0.2, respectively. The production of high-energy neutrons relies critically on two parameters: the energy of projectiles and Q-value of the reaction. Under non-relativistic limit, the energy of the emitted neutrons can be determined kinetically if these parameters and the angle of the emitted neutron are known, as long as there are no nuclear states excited in the resultant nuclei,

$$E_{\bar{c}} = [\frac{m_a m_{\bar{c}}}{(m_{\bar{c}}+m_{\bar{d}})^2} + \frac{m_b m_{\bar{d}}}{(m_a+m_b)(m_{\bar{c}}+m_{\bar{d}})}]E_a + \frac{m_{\bar{d}}Q}{m_{\bar{c}}+m_{\bar{d}}} + \sqrt{\frac{4\cos^2(\theta)m_a m_b m_{\bar{c}} m_{\bar{d}}}{(m_a+m_b)(m_{\bar{c}}+m_{\bar{d}})^3}(E_a^2 + \frac{m_a+m_b}{m_b}QE_a)}. \quad (19)$$

For D(D,n)^{3}He beam-target fusion, we have $m_a = 3672$, $m_b = 3672$, $m_{\bar{c}} = 1836$, $m_{\bar{d}} = 5508$. $E_a = 2.34$, 9.34, and 37.08 when the momentum of projectile is 0.05, 0.1 and 0.2 respectively. The black curve on Fig. 4 (a), (b) and (c) is the plot of Eq. 19. As we can see, under non-relativistic cases, our simulation results and analytical solution agree quite well. For relativistic velocities, as the analytical solution is not legible, numerical simulation is therefore is of great value.

IV. DISCUSSIONS AND CONCLUSIONS

To summarize, a pairwise nuclear fusion algorithm for particle-in-cell simulations for arbitrarily weighted macro-particles at relativistic energies is proposed. When comparing with a recent work by D. P. Higginson et al, our method is also fitted with the widely used Coulomb scattering algorithm by Takizuka and Abe, Nanbu and Yonemura, and Sentoku and Kemp. As the pairing scheme accounts for the entire macro-particle ensemble, the convergence of our method is therefore of quite robust. The algorithm is benchmarked in situations with like-particles, unlike-particles, thermonuclear plasmas, and beam-target fusion. It is shown that only $10 \sim 100$ macro-particle per cell is needed for the repeatability of fusion yields around 1%.

ACKNOWLEDGMENTS

Dr. D. Wu thanks Dr. Y. T. Zhao and Dr. L. Q. Shan for encouraging me to focus on nuclear-fusion algorithm for a couple of weeks. Help to analyse experimental data of neutron yields at Shenguang laser facilities is the main

motivation of doing this work. This work was supported by the Strategic Priority Research Program of Chinese Academy of Sciences (Grant No. XDA250050500) and Science Challenge Project (No. TZ2016005).

[1] C. K. Birdsall, A. B. Langdon, Plasma Physics via Computer Simulation, Taylor and Francis, New York, 2005.
[2] X. R. Jiang, F. Q. Shao, D. B. Zou, M. Y. Yu, L. X. Hu, X. Y. Guo, T. W. Huang, H. Zhang, S. Z. Wu, G. B. Zhang, T. P. Yu, Y. Yin, H. B. Zhuo and C. T. Zhou, Nucl. Fusion 60, 076019 (2020).
[3] Drew Pitney Higginson, Anthony Link, Andrea Schmidt, Journal of Computational Physics 388, 439 (2019).
[4] T. Takizuka, H. Abe, J. Comput. Phys. 25 205 (1977).
[5] K. Nanbu, S. Yonemura, Journal of Computational Physics 145 639 (1998).
[6] Y. Sentoku, A. J. Kemp, Journal of Computational Physics 227, 6846 (2008).
[7] T. D. Arber, K. Bennett, C. S. Brady, A. Lawrence-Douglas, M. G. Ramsay, N. J. Sircombe, P. Gillies, R. G. Evans, H. Schmitz, A. R. Bell and C. P. Ridgers, Plasma Phys. Control. Fusion 57, 113001 (2015).
[8] D. Wu, X. T. He, W. Yu, and S. Fritzsche, Phys. Rev. E 95, 023207 (2017).
[9] D. Wu, X. T. He, W. Yu, and S. Fritzsche, Phys. Rev. E 95, 023208 (2017).
[10] D. Wu, W. Yu, S. Fritzsche, and X. T. He, Phys. Rev. E 100, 013207 (2019).
[11] D. Wu, W. Yu, Y. T. Zhao, D. H. H. Hoffmann, S. Fritzsche, and X. T. He, Phys. Rev. E 100, 013208 (2019).
[12] H. S. Bosch, G. M. Hale, Nuclear Fusion 32, 611 (1992).
[13] B. Appelbe, J. Chittenden, Plasma Phys. Control. Fusion 53, 045002 (2011).
[14] R. B. Theus, W. I. McGarry, L. A. Beach, Nucl. Phys. 80, 273 (1966).
[15] R. L. Schulte, M. Cosack, A. W. Obst, J. L. Weil, Nucl. Phys. A 192, 609 (1972).
[16] A. Krauss, H. W. Becker, H. P. Trautvetter, C. Rolfs, K. Brand, Nucl. Phys. A 465, 150 (1987).
[17] W. H. Press, S. A. Teukolsky, W. T. Vetterling, B. P. Flannery, Numerical Recipes in C++, Cambridge University Press, 2007.
[18] G. E. P. Box, M. E. Muller, The Annals of Mathematical Statistics 29, 610 (1958).
[19] W. Hormann, J. Leydold, ACM Transactions on Modelling and Computer Simulation 13, 347 (2003).